JOURNAL OF AIRCRAFT
Vol. 37, No. 4, July–August 2000

Design and Predictions for High-Altitude (Low Reynolds Number) Aerodynamic Flight Experiment

Donald Greer* and Phil Hamory†
NASA Dryden Flight Research Center, Edwards, California 93523
Keith Krake‡
Sparta, Inc., Edwards, California 93523
and
Mark Drela§
Massachusetts Institute of Technology, Cambridge, Massachusetts 02139

A sailplane being developed at NASA Dryden Flight Research Center will support a high-altitude flight experiment. The experiment will measure the performance parameters of an airfoil at high altitudes (70,000–100,000 ft), low Reynolds numbers (2×10^5–7×10^5), and high subsonic Mach numbers (0.5 and 0.65). The airfoil section lift and drag are determined from pitot and static pressure measurements. The locations of the separation bubble, Tollmien–Schlichting boundary-layer instability frequencies, and vortex shedding are measured from a hot-film strip. The details of the planned flight experiment are presented as well as several predictions of the airfoil performance.

Nomenclature

C_d = section drag coefficient
C_l = section lift coefficient
C_m = section moment coefficient
C_p = pressure coefficient
c = chord, ft
du = derivative of velocity, ft/s
dx = derivative of length, ft
e^n = amplitude ratio
g = force of gravity
M = Mach number
n_{crit} = critical amplification parameter
P = pressure, lb/ft^2
P_{max} = dimensionless pressure gradient
P_s = static pressure, lb/ft^2
P_T = total pressure, lb/ft^2
$\bar{q}$ = dynamic pressure, lbm · ft · s
Re = Reynolds number
U_x = uncertainty of the variable x
x_{tr} = transition location
α = angle of attack, deg
γ = ratio of specific heats
θ = momentum thickness
υ = kinematic viscosity, ft/s^2

Subscript

sep = separation

Presented as Paper 99-3183 at the AIAA 17th Applied Aerodynamics Conference, Norfolk, VA, 28 June–1 July 1999; received 5 August 1999; revision received 22 February 2000; accepted for publication 26 February 2000.

*Research Engineer, P.O. Box 273, M/S D2024. Member AIAA.
†Flight Instrumentation Engineer, P.O. Box 273, M/S D2138.
‡Flight Instrumentation Engineer, P.O. Box 273, M/S D2138. Member AIAA.
§Professor, Department of Aerospace Engineering. Member AIAA.

Introduction

THE need for cost-effective high-altitude vehicles to conduct atmospheric research has created interest in high-altitude (low Reynolds number) airfoils. In support of this need, NASA Dryden Flight Research Center is developing a sailplane called APEX that will measure the parameters affecting the performance of the airfoil in actual high-altitude flight. The APEX sailplane will be released from a high-altitude balloon from approximately 108,000-ft altitude and then be remotely piloted. Figure 1 shows a schematic of the flight mission.

The first 30 s after release from the balloon are the most critical for the APEX flight control system. Transition to horizontal flight occurs during this period with the assistance of four small rockets, which have a combined thrust of 784 lb. After the transition to horizontal flight, the airfoil parameters affecting performance are measured as the sailplane descends from 100,000 to 70,000 ft. The sailplane is then brought to a horizontal landing at the Rogers dry lakebed at Edwards Air Force Base, California.

Low Reynolds number airfoils typically exhibit laminar separation bubbles as shown schematically in Fig. 2. These separation bubbles are known to affect significantly the performance of an airfoil. The bubble is formed when the laminar flow separates as a result of encountering the adverse pressure region of the airfoil. The separated free shear layer is unstable, which amplifies the Tollmien–Schlichting instability waves. The free shear flow generally transitions rapidly from laminar flow to turbulent flow and then reattaches to the airfoil surface. The lambda shocks, which occur in the transonic flight regime, are expected to increase the amplification of the Tollmien–Schlichting instability waves.

The objectives of the APEX experiment are 1) to increase the understanding of airfoil performance in the high-altitude, low-Reynolds-number, and high-subsonic Mach number flight regime and 2) to obtain flight test data of airfoil performance parameters that can be used for validation of airfoil design codes.

Previous Research

Several studies investigating the performance and characteristics of low Reynolds number airfoils have been performed. Mueller[1] presents an excellent summary of the research before 1985. One interesting aspect that Mueller discusses is the hysteresis that often occurs in the drag polars. Mueller's wind-tunnel studies show that the airfoil performance, including the hysteresis, could be significantly affected by freestream turbulence and surface roughness. LeBlanc

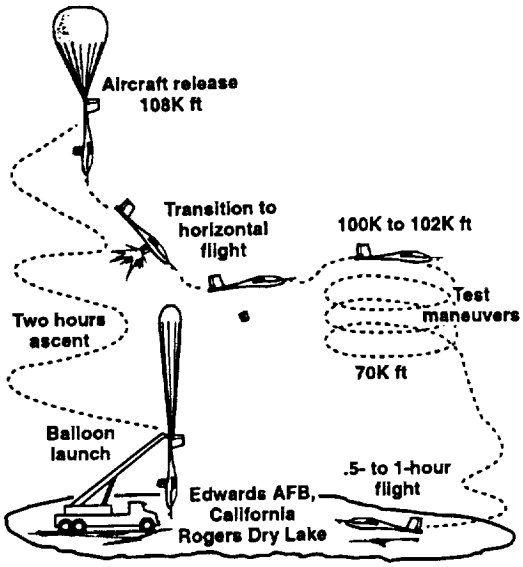

Fig. 1 APEX mission profile.

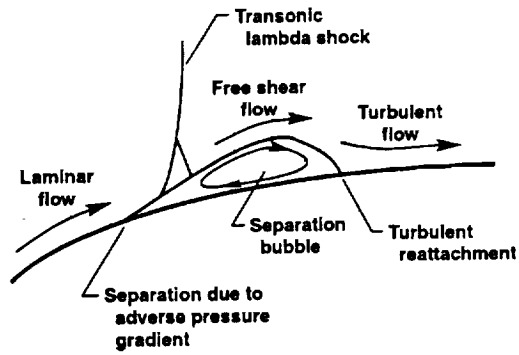

Fig. 2 Laminar separation bubble.

et al.[2] performed wind-tunnel measurements on a Liebeck airfoil at low Reynolds numbers. The boundary-layer velocity fluctuations in the separation bubble were measured with hot-wire anemometry. The measured velocity spectra of peak instability frequencies agreed with the predictions from linear stability theory analysis. Dovgal et al.[3] discuss several aspects of the instability associated with laminar separation bubbles including receptivity, linear instability, and nonlinear interactions.

Recent investigations of Pauley et al.,[4] Ripley and Pauley,[5] and Muti Lin and Pauley[6] show that the separation bubble may become unstable under certain conditions and experiences periodic vortex shedding. Their transient incompressible Navier–Stokes analytical studies characterized the unsteady vortex shedding structure. Tatineni and Zhong[7,8] performed a two-dimensional, time-accurate Navier–Stokes analysis on the APEX-16 airfoil flowfield. Their analysis indicates that the airfoil separation bubble is unstable and periodically sheds at the flight conditions of the APEX sailplane. A linear stability analysis also showed that the most dominant instability frequency matches the frequency of the periodic vortex shedding. Drela[9] investigated high-altitude, low Reynolds number airfoils in the transonic flight regime with the ISES code. An interesting aspect of this investigation is that airfoil performance in the high-altitude flight regime may depend largely on the effectiveness of lambda shocks to increase the amplification of instability waves and increase the transition rate in the separation bubble.

Turbulence is expected to be a major factor in the performance of the APEX-16 airfoil. The length of the separation bubble depends on the growth of the instability waves within the free shear layer and transition to fully developed turbulence. Although the receptivity process to transition is difficult to quantitatively predict, it is well known to be a strong function of freestream turbulence as shown by Dryden and Kuethe[10] and Dryden et al.[11] in several experiments measuring the critical Reynolds number of a sphere as a function of freestream turbulent intensity. Presently, no existing wind tunnel can provide the high-altitude (70,000–100,000 ft), low Reynolds number (2×10^5–7×10^5), high-subsonic Mach number (0.5–0.65), and low-freestream turbulent-intensity (0.02% or less) environment necessary to accurately measure the APEX-16 airfoil performance. Natural atmospheric turbulence is the rationale for constructing the APEX research sailplane and measuring the in-flight airfoil performance parameters rather than performing a wind-tunnel study.

APEX Sailplane Description

Murray et al.[12] originally proposed the APEX sailplane as a modified Schweizer SGS 1-36 sailplane. As the APEX design proceeded, the sailplane evolved into the current configuration. Figure 3 shows the APEX sailplane geometry. The sailplane is 22.7 ft long with a wingspan of 41.2 ft and has a wing aspect ratio of 13.6. The experimental test section, where the performance parameters are measured, is at the midspan point of the right wing as shown in Fig. 3. The sailplane is designed for a target gross weight of 600 lb with a 5-g maneuver load factor.

The APEX-16 airfoil was designed using the coupled viscous/inviscid MSES code.[13,14] The airfoil shape is shown in Fig. 4. The airfoil dimensional tolerances for the wing construction are specified at ±0.005 in. to reduce the effects of surface roughness and waviness. The wing is a rectangular planform of the APEX-16 airfoil, as was shown in Fig. 3. The wing incorporates a 2-deg linear wash-in to reduce three-dimensional (spanwise) effects and to provide a more uniform section lift coefficient (C_l) distribution over the experimental area of the wing. Figure 5 shows the predicted APEX flight envelope. The challenge of the design was to predict correctly the characteristics of the separation bubble without experimental data for code verification in the high-subsonic Mach number and low Reynolds number flight regime.

The experiment is limited by several design constraints. Weight is a major design consideration for the experiment. The gross vehicle

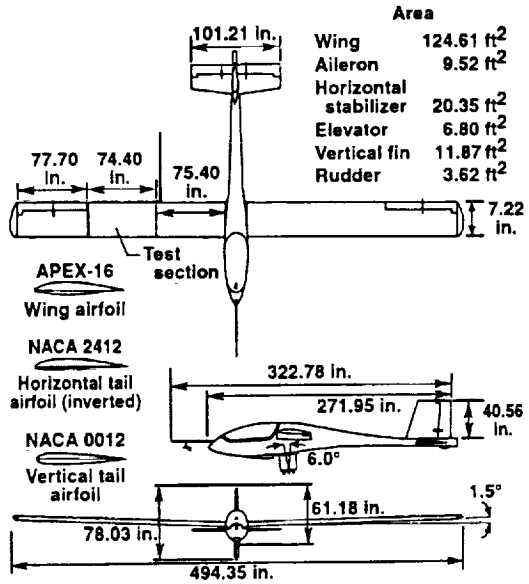

Fig. 3 APEX three-dimensional view.

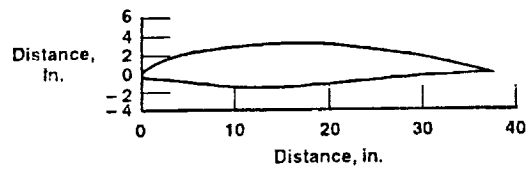

Fig. 4 APEX-16 sectional (37.22-in. chord).

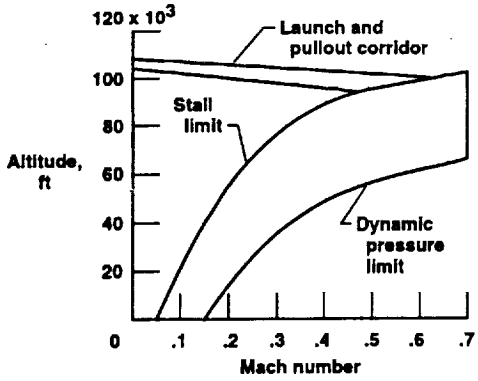

Fig. 5 APEX flight envelope.

flight weight for the sailplane is specified at 600 lb to provide an adequate stall margin for attaining a ceiling altitude of 100,000 ft. The experiment is limited to 10% of the gross vehicle weight or 60 lb. Packaging the experiment is also another major design constraint. Much of the instrumentation electronics, including pressure transducers, accelerometers, and the hot-film anemometry, signal conditioning, and A/D conversion cards, are in the wing next to the experiment. The electronic instrumentation is located close to the experiment to minimize noise from radio frequency interference and electrical magnetic interference. The wing chord is 37.22 in. with a maximum interior thickness of 5 in., which makes instrumentation packaging difficult. Another design constraint is the high altitude. The available off-the-shelf instrumentation that can provide adequate range and accuracy at high altitude is limited. Some instrumentation had to be specifically designed for the experiment. The air density at 100,000-ft altitude is approximately 1% of its value at sea level, which substantially lowers the convective cooling rates of the electronics to the air. Some electronics require a specialized cooling design to avoid overheating.

APEX Experimental Description

The flight experiment to measure the performance parameters of the APEX-16 airfoil consists of three primary measurements:

1) First, to measure section lift, a series of static pressure taps circle the airfoil at one spanwise location.

2) Second, to measure section drag, a trailing rake sits behind the airfoil with a support sting.

3) Third, to measure the separation bubble location, Tollmien–Schlichting frequencies, and vortex shedding, a hot-film strip sits on the top surface of the airfoil.

Figure 6 presents a schematic layout of the airfoil instrumentation. In addition to the primary measurements, the instrumentation also includes a Kiel probe to measure freestream total pressure, a trailing static probe to measure freestream static pressure, a boundary-layer rake to determine the velocity profile, a total temperature measurement, five integrating boundary-layer rakes to determine the section drag developing over the upper surface, two integrating trailing rakes to determine total section drag, three accelerometers to measure wing surface vibration, and two vanes mounted on the noseboom to measure angles of attack and sideslip.

Pressure Measurement System

Figure 7 presents a schematic of the pneumatic pressure measurement system. Along the chord, 50 static pressure ports (30 on the upper surface and 20 on the lower surface) measure the pressure distribution over the airfoil. The ports have a 0.05-in. diam and are staggered at a 15-deg angle relative to the chord to prevent contamination from upstream ports. A trailing rake comprises 26 total pressure probes and 3 static probes to determine section drag C_d. The rake is mounted 0.3 chord length aft of the airfoil where the static pressure is expected to be fully recovered.

The airfoil section drag is calculated from the rake pressures based on the Jones[15] method corrected for compressibility effects.

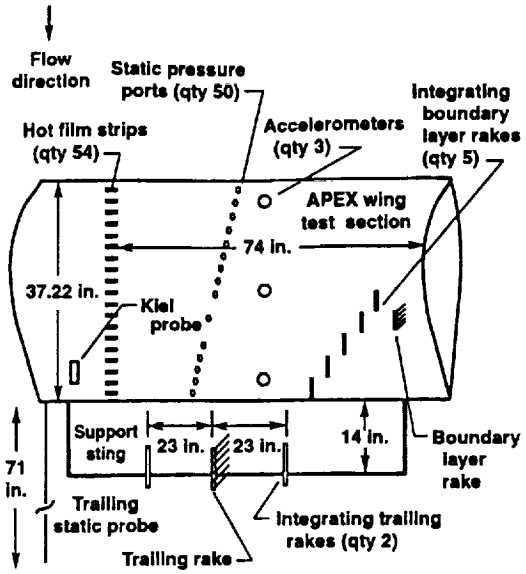

Fig. 6 APEX instrumentation layout on right-wing test section.

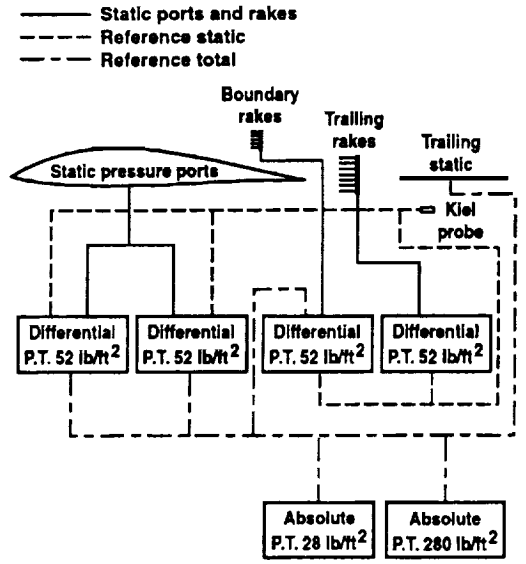

Fig. 7 Pneumatic pressure measurement system for the right-wing test section.

A Kiel probe, located midchord, 8 in. from the lower surface of the airfoil, measures a reference total pressure P_T. A trailing static probe, placed three chord lengths aft of the airfoil, measures a reference static pressure P_s. A conventional boundary-layer rake placed at 70% chord determines the boundary-layer velocity profile development on the upper surface. Five integrating boundary-layer rakes are located at 60, 70, 80, 90, and 100% chord, and two integrating trailing rakes are located at 0.3 chord lengths aft of the airfoil. The integrating rakes are multipitot probe rakes, such as those developed by Silverstein and Katzoff,[16] in which the pitot probes are plumbed into a common reservoir for a single average total pressure measurement. The average total pressure measurement has been shown to be a direct determination of the sum of momentum thickness and displacement thickness from which drag can be calculated.

Uncertainty Analysis

A preliminary measurement uncertainty analysis was performed on the pressure system and is summarized with a discussion of the bias error for the calculation of lift. This analysis is based on the general uncertainty analysis of Coleman and Steele.[17] The pressure

coefficient C_p can be defined in terms of measured quantities as follows:

$$C_p = \frac{P - P_s}{\bar{q}} = \frac{P - P_s}{0.7P_sM^2}$$

$$= \frac{P - P_s}{0.7P_s[2/(\gamma - 1)]\left[(P_T/P_s)^{(\gamma-1)/\gamma} - 1\right]} \quad (1)$$

Treating $P - P_s$, P_s, and P_T/P_s as measured quantities, the general uncertainty equation is

$$\left(\frac{U_{C_p}}{C_p}\right)^2 = \left(\frac{U_{P-P_s}}{P - P_s}\right)^2 + \left(\frac{U_{P_S}}{P_S}\right)^2$$

$$+ \left\{\frac{U_{P_T}/P_s[\gamma/(\gamma - 1)](P_T/P_s)^{(\gamma-1)/\gamma}}{\left[(P_T/P_s)^{(\gamma-1)/\gamma} - 1\right]}\right\}^2 \quad (2)$$

where U is the uncertainty for the subscript variable.

For a $C_p = 1$, a flight condition of Mach 0.65, and 100,000-ft altitude, the expected pressure coefficient bias error is

$$C_p = 1 \pm 0.02 \quad (3)$$

The bias error for the section lift coefficient,

$$C_l = \frac{1}{c}\int_0^c \left(C_{p_l} - C_{p_u}\right) dx \quad (4)$$

is expected to be

$$C_l = 0.9 \pm 0.028 \quad (5)$$

A similar bias error analysis for the calculation of the section drag coefficient for the flight condition of Mach 0.65 and 100,000-ft altitude yields

$$C_d = 0.02 \pm 0.004 \quad (6)$$

The percentage of bias error decreases as the sailplane descends to lower altitudes because the measured pressures become larger. For a $C_p = 1$ and a flight condition of Mach 0.65 and 70,000-ft altitude, the expected bias errors are

$$C_p = 1 \pm 0.005 \quad (3a)$$

$$C_l = 0.9 \pm 0.006 \quad (5a)$$

$$C_d = 0.01 \pm 0.0005 \quad (6a)$$

Hot-Film Measurement System

A multi-element hot-filmstrip is mounted over the APEX-16 airfoil. The hot-filmstrip measures the state of the boundary layer (i.e., laminar boundary layer, laminar separation, bubble region, turbulent reattachment, turbulent boundary layer, turbulent separation, and vortex shedding) and the frequency of the Tollmien–Schlichting instability waves in the separation bubble. The strip consists of 50 hot films on the top surface in 2% chord increments starting at 0% chord. The hot films are spaced approximately 0.75 in. apart. In addition, four hot films are placed on the bottom surface at 10, 30, 60, and 90% chord. This hot-filmstrip configuration is used for the initial flights. After the separation bubble is located for the APEX flight regime, the strip is replaced with a denser strip concentrated in the area of the separation bubble (approximately 50 evenly spaced hot films on a 15% chord length).

The desire to obtain valid hot-film anemometry data at frequencies up to 10 kHz, combined with the weight and packaging limitations, significantly influenced the design. The APEX telemetry system cannot handle these high data transfer rates for the large number of channels. Therefore, the data are stored onboard in random access memory and later, after the high-altitude tests are completed, sent by telemetry to the ground at lower data transfer rates. The hot-film data are split into two components: a dc component and an ac component. The dc component is sampled at 200 Hz and sent by telemetry to the ground in real time. The ac component is sampled in 1-s data intervals at 20–25 kHz and stored in memory. The system is capable of storing up to 10, 1-s data intervals during a flight. The system is commanded from the ground uplink to begin storing a 1-s data interval of ac data. In summary, all 54 hot films are sampled for their dc component at 200 Hz as the sailplane descends from 100,000 to 70,000 ft. The 54 hot films are sampled for their ac component at 20–25 kHz in 1-s data intervals for up to 10 intervals as the sailplane descends from 100,000 to 70,000 ft.

Spectral analysis is the primary means of data reduction of the hot-film data. Preliminary calculations show that a 1-s interval of data sampled at 20–25 kHz is adequate to resolve the spectral content between 50 Hz and 10 kHz. This spectral content should be adequate for determining the flowfield on the upper surface of the APEX airfoil. The detection of phase reversal and a significant change in power spectral density is expected to be the signature of laminar separation and the beginning of the separation bubble. Phase reversal of low-frequency spectra has been shown by Mangalam et al.[18] to be an effective method of detecting laminar separation.

Turbulent reattachment of the bubble is detected in the same manner as laminar separation: by phase reversal and a significant change in power spectral density caused by turbulence. The presence of vortex shedding is detected by performing both auto- and crosspower spectral density analysis on the hot films aft of the separation bubble. The detection of a significant increase in spectra in a specific frequency range and a consistent phase lag between the hot films is a signature of vortex shedding.

The Tollmien–Schlichting instability wave frequencies in the free shear layer of the bubble are detected by spectral analysis of hot films inside the separation bubble and possibly by hot films just upstream of the separation bubble. The separated flow instability research of Dovgal et al.[3] show that instability waves, which cause transition, can be generated either upstream of the separation point or downstream of the separation point in the free shear layer. Their experiments show that harmonic disturbances causing transition exist inside the separation bubble. They discuss the concept of feedback interactions whereby instability waves are convected forward to the separation point as the flow circulates inside the bubble.

At present, hot films have not been used to detect Tollmien–Schlichting instability frequencies, and the bubble instabilities are assumed to be detected at the surface of the airfoil. The computational fluid dynamics analysis and Orr–Sommerfeld analysis performed by Tatineni and Zhong[7,8] suggest that the Tollmien–Schlichting instability waves occur at approximately 1000 Hz. A significant increase in the spectral density in this frequency range for hot films in the separation bubble is, therefore, a measure of the Tollmien–Schlichting instability frequencies.

Uncertainty Analysis

Before actual flight, any estimate of the data quality from the hot-film system is difficult. The goal is a signal-to-noise ratio of 20 or greater. To reduce radio frequency interference and electrical magnetic interference noise, the hot-filmstrip comprises three laminated sheets. The top and bottom sheets are ground planes to shield the hot-film leads in the middle sheet. Twisted and shielded cabling are used for connections. The anemometry cards are packaged with ground plane protection.

The aircraft power is filtered to ensure that the anemometry signals are not contaminated by power fluctuations. Special preflight ground test equipment is being developed that selectively blows both laminar and turbulent air over each hot film, to match the Nusselt number expected in flight. This equipment allows the individual hot-film signals to be compared and used to qualify, to first order, signal intensities between hot films. In addition, while the sailplane is suspended under the balloon, a 1-s data interval is taken to assess noise levels.

Predicted Airfoil Performance

The prediction of low-Reynolds-number airfoil performance is a formidable task that involves correctly modeling several flow phenomena, as was shown in Fig. 2. Modeling the inviscid flow field, including the presence of shock waves, is generally considered the

first step to determining the pressure distribution over the surface of the airfoil. The viscous flowfield is composed of the boundary layer, laminar separation, laminar-free shear layer, transition to turbulence in the free shear layer, turbulent-free shear layer, reattachment of the turbulent-free shear layer, and turbulent boundary layer. In addition turbulent separation and laminar bubble separation, known as bubble bursting, are important physical characteristics to be modeled. The interaction between the inviscid and viscous flowfields can be significant. The presence of the separation bubble alters the effective shape of the inviscid airfoil. The classic assumption that pressure is constant across the boundary layer may not be valid across the separation bubble. In addition, boundary layers become large at low Reynolds numbers and increase the boundary displacement thickness, which can have an appreciable effect on the inviscid pressure distribution.

The design and initial predictions of the APEX-16 airfoil are performed with the MSES code. The MSES airfoil design code uses the Euler equations to solve the inviscid flowfield coupled with a two-equation dissipation integral method to solve for the viscous boundary layer. The transition location is determined via the amplitude ratio e^n method, by the use of growth rates that are precomputed from solutions of the Orr–Sommerfeld equation and correlated to the local shape-factor parameter and momentum-thickness Reynolds number. No compressibility corrections are employed, partly because of the large uncertainty in the appropriate critical amplification parameter for this high-subsonic-Mach number and low Reynolds number flight regime. A value of 12 for n_{crit} was assumed for design of the APEX-16 airfoil. Liebeck[19] uses an earlier version of the MSES code, ISES, and finds that the predictions for low Reynolds number airfoils are reliable and accurate for low Mach numbers. One goal of the APEX experiment is to determine whether MSES remains reliable in the high-subsonic Mach number and low Reynolds number flight regime and what n_{crit} values are appropriate.

Figure 8 presents the predicted drag polars and lift curves for the APEX-16 airfoil for the chord Reynolds number of 2×10^5; Fig. 9 presents the predicted drag polars and lift curves for various chord Reynolds numbers between 2×10^5 and 2×10^6 for a 0.6 Mach number. The first apparent characteristic in Figs. 8 and 9 is the decrease in maximum lift coefficient with increasing Mach number. This decrease results from the separation of the turbulent boundary layer from the airfoil as the Mach number increases. The maximum lift coefficient decreases and the drag coefficient increases as the Reynolds numbers decrease. This result is expected as the separation bubbles become larger with lower Reynolds numbers, which decreases the overall performance of the airfoil. The lift curve slope is relatively unaffected by Mach number and Reynolds number except near stall. The slope of the pitching moment coefficients with angle of attack is also relatively unaffected by Mach number and Reynolds number. The predicted transition locations x_{tr} vs lift coefficient are also presented in Figs. 8 and 9. The transition location on the upper surface moves forward and the transition location on the lower surface moves aft with increasing lift coefficient or angle of attack. Figure 10 shows the APEX-16 airfoil predicted pressure distribution for Reynolds numbers of 2×10^5 and 3×10^5 at Mach 0.65.

A time-accurate Navier–Stokes analysis was performed on the APEX-16 airfoil by Tatineni and Zhong.[7,8] Their analysis predicts that the separation bubble on the upper surface of the airfoil is unstable. The separation bubble is predicted to shed periodically at about 950 Hz for the subsonic flight condition of Mach 0.5, Reynolds number 2×10^5, and an angle of attack of 4 deg. The flowfield over the upper surface is predicted to become very erratic as the Mach number is increased into the transonic range, as shown in Figs. 11

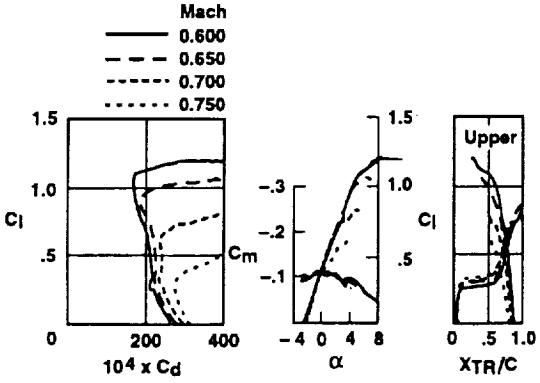

Fig. 8 MSES prediction for APEX-16 airfoil at $Re = 2 \times 10^5$.

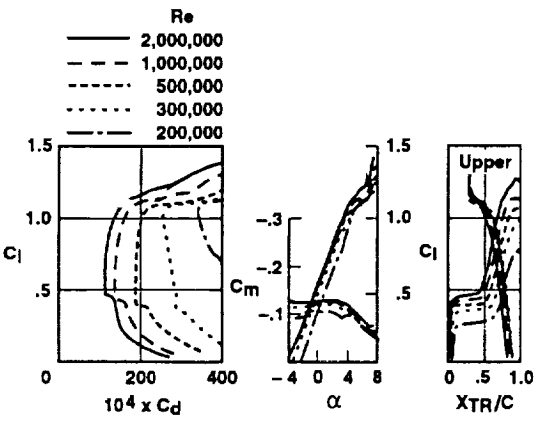

Fig. 9 MSES prediction for APEX-16 airfoil at $M = 0.6$.

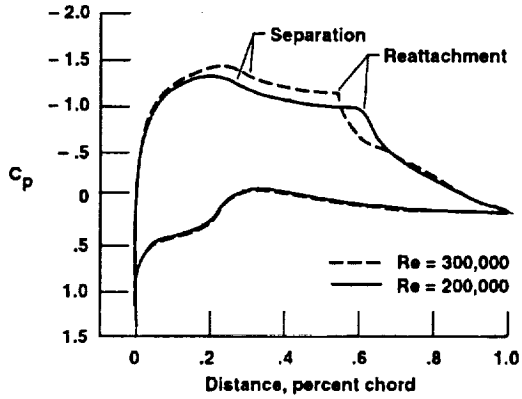

Fig. 10 MSES prediction of the pressure distribution over the APEX-16 airfoil ($M = 0.65$, $\alpha = 3.5$ deg, and $Re = 2 \times 10^5$ and 3×10^5).

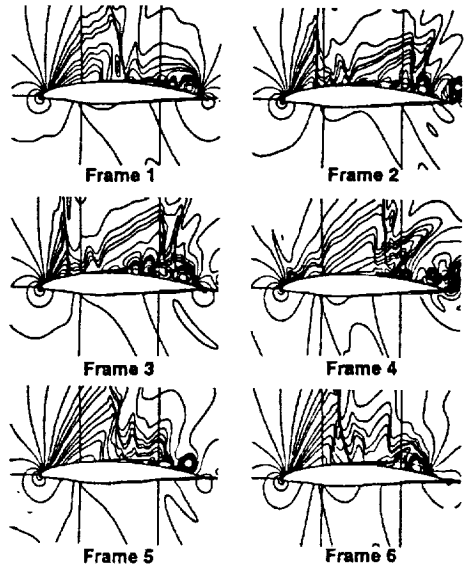

Fig. 11 Unsteady variation of pressure contours for the transonic APEX-16 airfoil ($M = 0.65$, $Re = 2 \times 10^5$, and $\alpha = 4$ deg); time interval between frames is 0.0016 s.

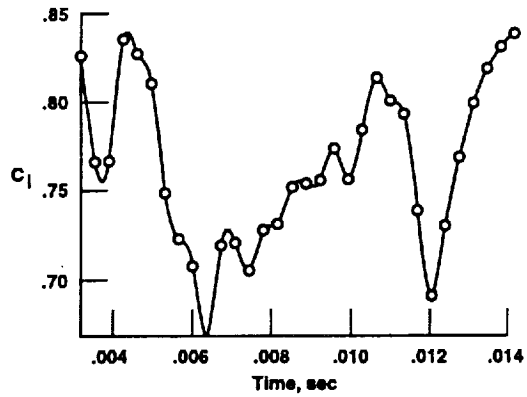

Fig. 12 Unsteady variations of average section lift coefficient for the transonic APEX-16 airfoil ($M = 0.65$, $Re = 2 \times 10^5$, and $\alpha = 4$ deg).

and 12. The predicted interaction between the shock waves and the shedding vortices, as seen in Figs. 11 and 12 has a profound effect on the flowfield and the airfoil section lift coefficient. The section drag also increases substantially.

The vortex shedding criterion suggested by Pauley et al.[4] is

$$P_{\max} = \frac{\theta_{\text{sep}}^2}{\upsilon}\left(\frac{\mathrm{d}u}{\mathrm{d}x}\right)_{\max} \approx -0.24 \tag{7}$$

The shedding criterion for the APEX-16 airfoil at a flight condition of Mach 0.65, Reynolds number 2×10^5, and an angle of attack of 4 deg is

$$P_{\max} = -1.47 \tag{8}$$

Therefore, unstable shedding vortices should be expected on the APEX-16 airfoil according to the suggested shedding criterion.

The stability of the separation bubble has a large effect on the airfoil predicted performance. The MSES code, based on stable bubble calculations, predicts a lift coefficient of 0.96 at the flight condition of Mach 0.65, Reynolds number 2×10^5, and an angle of attack of 4 deg. The Navier–Stokes code predicts an average section lift coefficient of 0.76 for the same flight condition. The Navier–Stokes analysis assumed laminar flow. The effects of turbulence on the stability of the separation bubble are uncertain. Gruber et al.[20] performed a direct numerical simulation that showed that an amplified Tollmien–Schlichting wave in the free shear layer of a separation bubble develops into a large vortical structure. It is unknown whether the intensity of these vortical structures is large enough to maintain the structure as transition into turbulence occurs. These large vortical structures may be analogous to large-scale turbulent eddies that are quickly broken up in the turbulent flowfield through vortex stretching and the three-dimensional effects of turbulent flow.

Conclusion

The purpose of the APEX experiment is to increase the understanding of low-Reynolds-number airfoils in a low-turbulence flight environment. The APEX experiment regime is for altitudes between 70,000 and 100,000 ft, Mach numbers between 0.5 and 0.65, and Reynolds numbers between 10^5 and 7×10^5. The following characteristics of the airfoil are to be determined: 1) section lift, 2) section drag, 3) location of the separation bubble, 4) vortex shedding characteristics, and 5) Tollmien–Schlichting frequencies.

Acknowledgments

Appreciation is due Mahidhar Tatineni and Xiaolin Zhong of the UCLA Mechanical and Aerospace Engineering Department for their work done through NASA Dryden Flight Research Center and Grant NCC 2-374. The authors express their gratitude to the APEX project members developing the sailplane and experiment. We gratefully acknowledge Albion Bowers (NASA Dryden Flight Research Center, Edwards, California) and Richard Howard (Naval Postgraduate School, Monterey, California) for their many helpful discussions.

References

[1]Mueller, T. J., "Low Reynolds Number Vehicles," AG-288, AGARD, 1985.

[2]LeBlanc, P., Blackwelder, R., and Liebeck, R., "A Comparison Between Boundary Layer Measurements in a Laminar Separation Bubble Flow and Linear Stability Theory Calculations," *Low Reynolds Number Aerodynamics Conference Proceedings*, Springer-Verlag, Berlin, 1989, pp. 189–205.

[3]Dovgal, A. V., Kozlov, V. V., and Michalke, A., "Laminar Boundary Layer Separation: Instability and Associated Phenomena," *Progress in Aerospace Sciences*, Pergamon, Tarrytown, NY, Vol. 30, 1994, pp. 61–94.

[4]Pauley, L. L., Moin, P., and Reynolds, W. C., "The Stucture of Two-Dimensional Separation," *Journal of Fluid Mechanics*, Vol. 220, 1990, pp. 397–411.

[5]Ripley, M. D., and Pauley, L. L., "The Unsteady Structure of a Two-Dimensional Steady Laminar Separation," *Physics of Fluids, A*, Vol. 5, No. 12, 1993, pp. 3099–3106.

[6]Muti Lin, J. C., and Pauley, L. L., "Low-Reynolds-Number Separation on an Airfoil," *AIAA Journal*, Vol. 34, No. 8, 1996, pp. 1570–1577.

[7]Tatineni, M., and Zhong, X., "Numerical Simulation of Unsteady Low-Reynolds-Number Separated Flows Over Airfoils," AIAA Paper 97-1929, July 1997.

[8]Tatineni, M., and Zhong, X., "Numerical Simulations of Unsteady Low-Reynolds-Number Flows Over the APEX Airfoil," AIAA Paper 98-0412, Jan. 1998.

[9]Drela, M., "Transonic Low-Reynolds-Number Airfoils," *Journal of Aircraft*, Vol. 29, No. 6, 1992, pp. 1106–1113.

[10]Dryden, H. L., and Kuethe, A. M., "Effect of Turbulence in Wind Tunnel Measurements," NACA Rept. 342, 1929.

[11]Dryden, H. L., Schubauer, G. B., Mock, W. C., Jr., and Skramstad, H. K., "Measurements of Intensity and Scale of Wind-Tunnel Turbulence and Their Relation to the Critical Reynolds Number of Spheres," NACA Rept. 581, 1937.

[12]Murray, J., Moes, T., Norlin, K., Bauer, J., Geenen, R., Moulton, B., and Hoang, S., "Piloted Simulation Study of a Balloon-Assisted Deployment of an Aircraft at High Altitude," NASA TM-104245, Jan. 1992.

[13]Giles, M. B., and Drela, M., "Two-Dimensional Transonic Aerodynamic Design Method," *AIAA Journal*, Vol. 25, No. 9, 1987, pp. 1199–1206.

[14]Drela, M., and Giles, M. B., "Viscous-Inviscid Analysis of Transonic and Low-Reynolds-Number Airfoils," *AIAA Journal*, Vol. 25, No. 10, 1987, pp. 1347–1355.

[15]Jones, B. M., "The Measurement of Profile Drag by Pitot Traverse Method," Repts. and Memoranda 1688, Aeronautical Research Council, U.K., Jan. 1936.

[16]Silverstein, A., and Katzoff, S., "A Simplified Method for Determining Wing Profile Drag in Flight," *Journal of the Aeronautical Sciences*, Vol. 7, No. 7, 1940, pp. 295–301.

[17]Coleman, H. W., and Steele, W. G., Jr., *Experimentation and Uncertainty Analysis for Engineers*, Wiley, New York, 1989, pp. 40–116.

[18]Mangalam, S. M., Stack, J. P., and Sewall, W. G., "Simultaneous Detection of Separation and Transition in Surface Shear Layers," *Fluid Dynamics of Three-Dimensional Turbulent Shear Flows and Transition*, CP-438, AGARD, 1988, pp. 12-1–12-10.

[19]Liebeack, R. H., "Low Reynolds Number Airfoil Design for Subsonic Compressible Flow," *Low Reynolds Number Aerodynamics Proceedings*, Springer-Verlag, Berlin, 1989, pp. 314–330.

[20]Gruber, K., Bestek, H., and Fasel, H., "Interaction Between a Tollmien–Schlichting Wave and a Laminar Separation Bubble," AIAA Paper 87-1256, 1987.